

# Material design of indium based compounds: possible candidates for charge, valence, and bond disproportionation and superconductivity

Chang-Jong Kang<sup>1\*</sup> and Gabriel Kotliar<sup>1,2</sup>

<sup>1</sup>*Department of Physics and Astronomy, Rutgers University, Piscataway, New Jersey 08854, USA*

<sup>2</sup>*Condensed Matter Physics and Materials Science Department,  
Brookhaven National Laboratory, Upton, New York 11973, USA*

(Dated: January 11, 2019)

We design and investigate the physical properties of new indium compounds  $\text{AInX}_3$  ( $\text{A}$  = alkali metals,  $\text{X} = \text{F}$  or  $\text{Cl}$ ). We find nine new In based materials in their ground state that are thermodynamically stable but are not reported in ICSD (Inorganic Crystal Structure Database). We also discuss several metastable structures. This new series of materials display multiple valences, charge and bond disproportionation, and dimerization. The most common valence of In is  $3+$ . We also find two rare alternatives, one has  $\text{In}^{2+}$  with In-In dimerization and the other shows valence disproportionation to  $\text{In}^{1+}$  and  $\text{In}^{3+}$  with bond disproportionation. We study the possibility of superconductivity in these new In compounds and find that  $\text{CsInF}_3$  has a transition temperature about 24 K with sufficient hole doping and pressure.

## I. INTRODUCTION

Progress in theory and algorithms, coupled with increased computational power is now accelerating the discovery of new materials with useful physical properties. A notable recent success is the theory led discovery of high temperature superconductivity of hydrogen sulfide under pressure [1–5], which has set the record of the highest critical temperature reached so far. Other examples of recent predictions are existence of a metallic layer in a new family (112) of iron based superconductors [6–8], the prediction and synthesis of missing half-Heusler compounds [9–11], the prediction of new high-pressure phase materials such as  $\text{FeO}_2$  [12], calcium carbides [13], and  $\text{Na}_2\text{He}$  [14], which were also confirmed experimentally. For reviews see Refs. [15–20]. Theory and computation are thus beginning to play a decisive role in the search for new materials.

In this paper we apply material design methodology to find new indium halide compounds. There are multiple motivations for this study. One is the intrinsic interest in finding new mixed valent compounds, a condition that is very rare in the solid state, but has been a focus of interest for many years [21]. With an eye on possible applications, halide perovskites, such as  $\text{CsPbI}_3$  [22], are remarkable photovoltaic [23, 24] materials. They have also been studied as analogs, as they have very similar band structures [25, 26] of the high temperature superconductor  $\text{BaBiO}_3$  [27]. Another motivation is to make predictions in a new arena that will test a material design methodology, which assigns a likelihood that a material will form.

Indium compounds tend to form in an oxidation state of  $\text{In}^{3+}$ , and the valences  $\text{In}^{1+}$  and  $\text{In}^{2+}$  are not typical [28–30]. We find nine new indium fluoride/chloride compounds where indium is in a valence  $2+$  or  $1+$ ,

which have a very high probability to form within the framework of Adler *et al.* [31] and are thermodynamically stable within the density functional theory PBE (Perdew-Burke-Ernzerhof) functional. For a given composition we identify potential low-energy crystal structures for the indium fluoride/chloride compounds, as candidate structures and find the relation between the crystal structure and the valence state of indium. These indium fluoride/chloride compounds display multiple valences, charge and bond disproportionation, and indium-indium dimerization. The new indium fluoride/chloride compounds have too large of a band gap (of the order of  $\sim 4$  eV) to be useful for photovoltaic materials, but could be useful for other applications. In particular, hole-doped  $\text{CsInF}_3$  under pressure will exhibit superconductivity with transition temperature of 24 K.

## II. OUTLINE

In the beginning, we would like to summarize a material design workflow introduced in Ref. [31]. The material design process is initiated by the **qualitative ideas** including some physical idea of a model that one would like to explore or test, ways to enhance desirable physical properties of a material, and comparisons of a class of compounds that exhibit similar physical properties. The initial intuitions (zeroth order step) could be refined with simplified quantitative calculations using a model Hamiltonian or other computational tools like *ab initio* density functional theory (DFT). In this work, we have used DFT as a main computational tool to design a new material. Note that the “theoretical” material design workflow progresses in reverse order from experimental solid state synthesis.

The first step is the quantitative calculation of the **electronic structure**. It explores how to go from a well defined crystal structure of a material to the physical or chemical properties. The second step is the **prediction of the crystal structure** given a fixed chemical compo-

\* ck620@physics.rutgers.edu

sition. There are a number of structure prediction techniques [32] with DFT total energy calculations, and the prediction techniques require having an accurate method for calculating the total energy of a material at the DFT level. The third step is testing for **thermodynamic stability**: given the lowest energy crystal structure of the fixed composition, check whether it is stable against decomposition to all other compositions in the chemical system. The third step requires the knowledge of all other known stable compositions, their crystal structures and total energies, which is now facilitated by materials databases, such as Materials Project [33, 34], OQMD [35, 36], and AFLOWlib [37, 38]. Here, we have used the Materials Project database for analysis of thermodynamic stability and estimated the existence probability [31] based on the database.

Once the (thermodynamically) stable crystal structure is found, the electronic structure is calculated again with more elaborated DFT methods like hybrid functionals, the modified Becke-John (mBJ) exchange potential, and *GW* methods to obtain more accurate physical properties.

This paper is organized as follows: the detail computational method of each step for material design is provided in Sec. III. The computational results are presented in sequence of the material design workflow. Section IV A summarizes the initial qualitative idea (zeroth order step) and its validation (first step). The prediction of crystal structures (second step) of the indium halide compounds and their thermodynamic stabilities (third step) are presented in Sec. IV B and Sec. IV C, respectively. The details of electronic structures and superconducting properties (post-process) are provided in Sec. IV D. The paper closes with brief summary and conclusions in Sec. V.

### III. METHOD

#### A. Prediction of crystal structure

To obtain low-energy crystal structures of  $\text{AlInX}_3$  ( $\text{A}$  = alkali metals,  $\text{X}$  = F or Cl), we employed the *ab initio* evolutionary algorithm [39] implemented in USPEX [40] combined with DFT pseudopotential code VASP [41, 42]. The initial structures were randomly generated according to possible space groups. In these calculations, the structural optimization of all the newly generated structures were carried out by VASP with an energy cutoff of 520 eV and the exchange-correlation functional of generalized gradient approximation (GGA) of Perdew-Burke-Ernzerhof (PBE) [43] with the projector augmented wave (PAW) method [44, 45].

#### B. Thermodynamic stability

After the low-energy crystal structures were obtained, the corresponding total energies were calculated by us-

ing DFT pseudopotential code VASP [41, 42]. For the Brillouin-zone integration, an equal  $k$ -grid density was used for all materials by adopting the Monkhorst-Pack sampling grid with a reciprocal spacing of 64  $k$ -points per  $\text{\AA}^{-3}$ . We used the empirical correction schemes employed in Materials Project [31, 33, 46–49] to get an accurate formation energy. In addition, the Materials Project database was used for analysis of thermodynamic stability and the existence probability [31].

#### C. Electronic structure

The all-electron full-potential linearized augmented plane-wave (FP-LAPW) method implemented in WIEN2k [50] was adopted to calculate the electronic structure. The GGA(PBE) exchange-correlation functional was chosen to calculate the electronic structure. To get the precise band gap, we utilized the modified Becke-John (mBJ) exchange potential [51], which is rather accurate and computationally cheaper than the *GW* method. The Brillouin zone integration was done with a  $17 \times 17 \times 17$   $k$ -mesh and the plane-wave cutoff was  $R_{\text{mt}}K_{\text{max}} = 7$ . The maximum  $L$  value for the waves inside the atomic spheres,  $L_{\text{max}} = 10$ , and the largest  $G$  in the charge Fourier expansion  $G_{\text{max}} = 12$  were used in the calculations.

#### D. Phonon dispersion and electron-phonon coupling calculations

We used the linear response method [52] implemented in Quantum Espresso [53] for phonon calculations. All pseudopotentials used in the calculations were adopted from Standard Solid State Pseudopotentials [54, 55]. We used a  $10 \times 10 \times 10$   $k$ -grid and a Gaussian smearing of 0.03 Ry for the electronic integration. The dynamical matrices were calculated on a  $4 \times 4 \times 4$  phonon-momentum grid. A  $20 \times 20 \times 20$   $k$ -grid was used for the electron-phonon coupling calculations. The standard exchange-correlation functionals like local-density approximation (LDA) and generalized gradient approximation (GGA) neglect the long-range exchange interaction. This nonlocal correlation could play a significant role in electron-phonon interaction [56]. To incorporate the long-range exchange interaction, the Heyd-Scuseria-Ernzerhof hybrid functional (HSE06) [57] was used and the electron-phonon coupling constant was calculated from the HSE06 deformation potential introduced in Ref. [56].

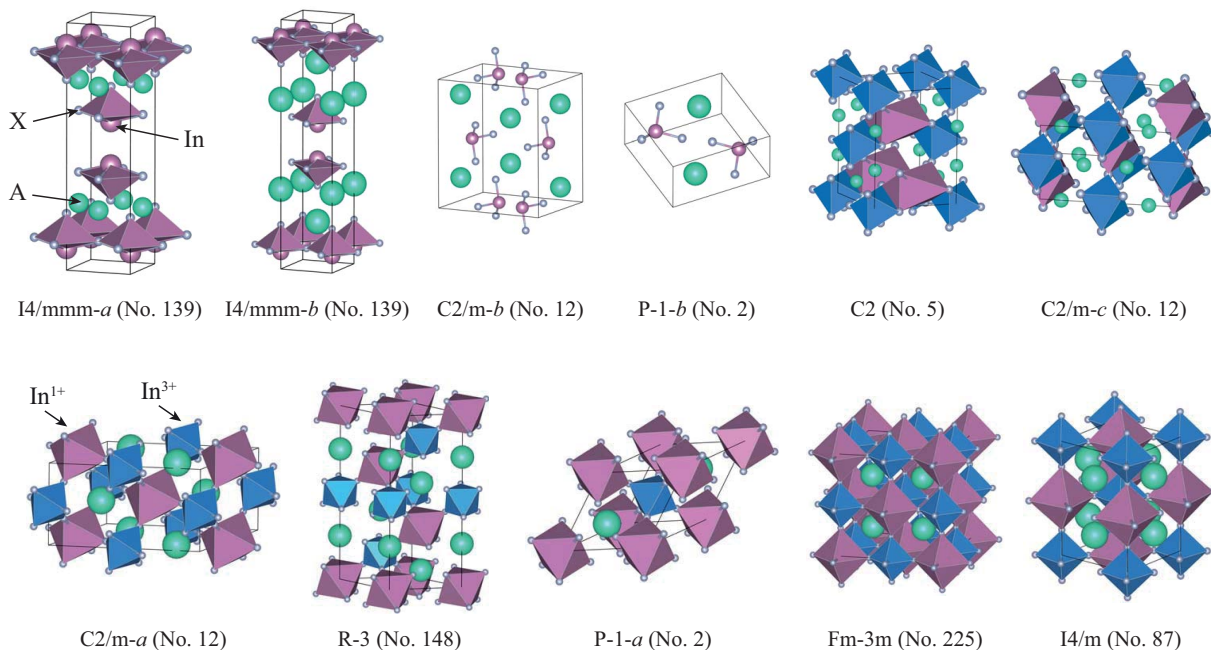


FIG. 1. (Color Online) Possible candidates for low-energy crystal structures of  $AInX_3$  ( $A$  = alkali metals,  $X$  = F or Cl) obtained by USPEX simulations. Space groups are also provided below for each crystal structure. Structures listed in the second row could be identified from structural distortions (breathing and/or tilting of  $InX_6$  octahedra) in the ideal cubic perovskite structure. For the structures, octahedra centered at  $In^{3+}$  or  $In^{1+}$  are colored in navy or pink, respectively. Letters  $a$ ,  $b$ , and  $c$  are attached to the end of the space group notation if different crystal structures have the same space group.

## IV. COMPUTATIONAL RESULTS AND DISCUSSION

### A. Initial idea and its validation

We conceived the idea that new indium halide compounds have physical and chemical similarities with  $BaBiO_3$  [27], a high temperature superconductor, and  $CsPbI_3$  [22], a high performance photovoltaic material. To justify the initial idea briefly, we assumed that new indium halide compounds have the ideal cubic perovskite structure. To get an unknown lattice constant of the perovskite structure, we performed the structural relaxation with VASP. After obtaining the relaxed crystal structures for the indium halide compounds, the electronic structures were obtained from the DFT calculations. Comparing the electronic structures, we could conclude that indium halide compounds have similar physical properties to the ones exhibited in  $BaBiO_3$  and  $CsPbI_3$ . Therefore, indium halide compounds could be possible candidates for high-temperature superconductors or photovoltaic materials.

### B. Crystal structure and total energy profile

The possible candidates for low-energy crystal structures of  $AInX_3$  ( $A$  = alkali metals,  $X$  = F or Cl) obtained by USPEX are summarized in Fig. 1 [58].

The crystal structures having the lowest energy are tetragonal structures with space group  $I4/mmm$  (No. 139) for  $AInF_3$  ( $A$  = Li, Na, K, and Rb) (see Fig. 2) however, Wyckoff sites for  $A$  are different:  $4d$  for both Li and Na, and  $4e$  for both K and Rb. Therefore, we have labeled the space group  $I4/mmm$  having two different Wyckoff sites  $4d$  and  $4e$  with  $I4/mmm-a$  and  $I4/mmm-b$ , respectively, in order to distinguish different crystal structures with the same space group. The coordination number of In in  $I4/mmm-AInF_3$  ( $A$  = Li, Na, K, and Rb) is 5 that makes a  $InF_5$  pyramid (Fig. 1). Alkali metals  $A$  and F strongly have 1+ and 1- valence states, respectively, hence, In should have 2+ valence state in order for the system to be charge neutral. The 2+ valence state for In is very unique because In usually has 3+ valence state.

For  $CsInF_3$ , five space groups,  $C2/m-a$ ,  $R\bar{3}$ ,  $P\bar{1}-a$ ,  $Fm\bar{3}m$ , and  $I4/m$  are candidates for the lowest energy structure and have tiny energy differences within 1 meV/atom (which corresponds to  $\sim 10$  K in temperature) to each other (Fig. 2). The details of the energy differences could be found in Table I. They could be identified from structural distortions (breathing and/or tilting of  $InF_6$  octahedra) in the ideal cubic perovskite structure and have different sizes of  $InF_6$  octahedra (Fig. 1). One has short In-F bond length ( $\sim 2.12$  Å) and it leads for In having 3+ valence state. On the other hand, the other has long In-F bond length ( $\sim 2.68$  Å) and it results in In 1+ valence state. Therefore, the different In-F bond

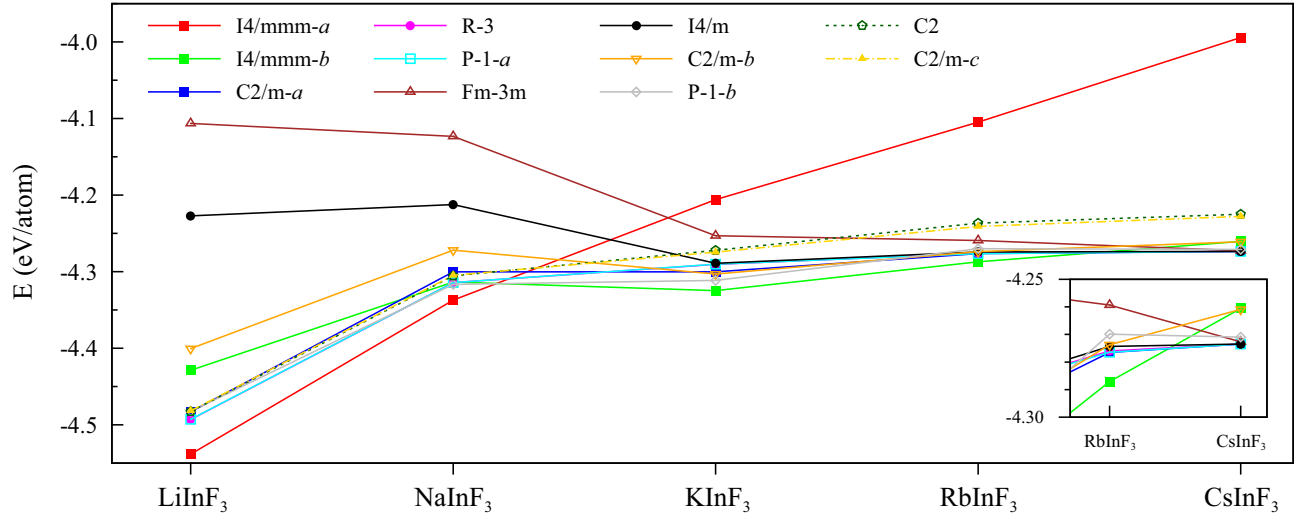


FIG. 2. (Color Online) Total energies of crystal structures listed in Fig. 1 for  $\text{AInF}_3$  ( $A = \text{alkali metals}$ ). Inset is provided to zoom in for nearly degenerate phases of  $\text{RbInF}_3$  and  $\text{CsInF}_3$ . The space group  $I4/mmm-a$  is the ground state crystal structure for both  $\text{LiInF}_3$  and  $\text{NaInF}_3$ , and  $I4/mmm-b$  is for both  $\text{KInF}_3$  and  $\text{RbInF}_3$ . For  $\text{CsInF}_3$ , five space groups ( $C2/m-a$ ,  $R\bar{3}$ ,  $P\bar{1}-a$ ,  $Fm\bar{3}m$ , and  $I4/m$ ) are candidates for the lowest energy structure and are almost degenerate. The energy differences among the five space groups are within 1 meV/atom.

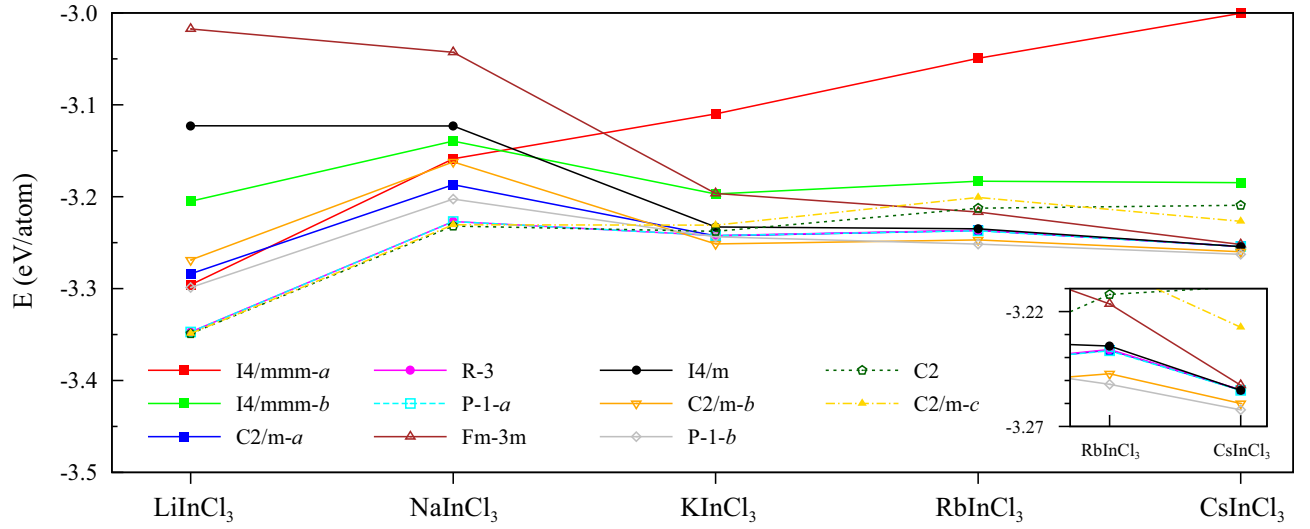


FIG. 3. (Color Online) Total energies of crystal structures listed in Fig. 1 for  $\text{AInCl}_3$  ( $A = \text{alkali metals}$ ). Inset is provided to zoom in for nearly degenerate phases of  $\text{RbInCl}_3$  and  $\text{CsInCl}_3$ . Four space groups,  $R\bar{3}$ ,  $P\bar{1}-a$ ,  $C2$ , and  $C2/m-c$ , are candidates for the lowest energy structure of  $\text{LiInCl}_3$  and  $\text{NaInCl}_3$ , and energy differences among the four space groups are within 5 meV/atom. For  $\text{KInCl}_3$ ,  $\text{RbInCl}_3$ , and  $\text{CsInCl}_3$ , two space groups,  $C2/m-b$  and  $P\bar{1}-b$ , are candidates for the lowest energy structure, and energy differences between the two space groups are within 9 meV/atom.

lengths (bond disproportionation) trigger charge/valence disproportionation. We would like to note that the crystal structure of  $\text{CsInF}_3$  with the space group  $C2/m-a$  is quite similar to that of  $\text{BaBiO}_3$ , which has also the monoclinic structure with a space group  $C2/m$  at low temperature [59–61]. For  $\text{BaBiO}_3$ , the Bi atoms occupy two distinct Wyckoff sites with average Bi-O distances of 2.28 and 2.12 Å, respectively [59], which results in valence disproportionation of  $\text{Bi}^{3+}$  and  $\text{Bi}^{5+}$  [61, 62].

The crystal structure with the space group  $I4/mmm-a$  has the lowest energy for  $\text{LiInF}_3$  and  $\text{NaInF}_3$ , however, it has higher energy as the alkali metal gets heavier as shown in Fig. 2. The other crystal structures listed in Fig. 1 have significant energy differences among them in  $\text{LiInF}_3$  but these energy differences become smaller as the alkali metal becomes heavier. For  $\text{CsInF}_3$ , these energy differences are within 13 meV/atom and energy differences among five candidate structures (with space

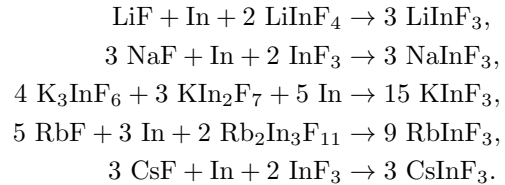


groups  $C2/m-a$ ,  $R\bar{3}$ ,  $P\bar{1}-a$ ,  $Fm\bar{3}m$ , and  $I4/m$ ) are only within 1 meV/atom. The energy difference between the lowest and the next lowest energy is gradually reduced as the alkali metal becomes heavier: 45, 20, 13, 11, and 0.01 meV/atom for Li, Na, K, Rb, and Cs compounds, respectively (see Table I). Judging from these energy differences,  $\text{AlInF}_3$  is likely synthesized into the space group  $I4/mmm-a$  for both Li and Na and  $I4/mmm-b$  for both K and Rb compounds if they are thermodynamically stable (their thermodynamic stabilities will be discussed later on). However, synthesis of  $\text{CsInF}_3$  quite depends on the synthesis method and condition due to the quite small energy difference. It could be one of five candidate structures (with space groups  $C2/m-a$ ,  $R\bar{3}$ ,  $P\bar{1}-a$ ,  $Fm\bar{3}m$ , and  $I4/m$ ) depending on the synthesis condition. Or otherwise, it exists in several different polymorphs. Note that charge-ordered thallium halide perovskites  $\text{CsTiX}_3$  ( $X = \text{F}$  or  $\text{Cl}$ ) are successfully synthesized.  $\text{CsTiF}_3$  has a cubic phase ( $Fm\bar{3}m$ ). On the other hand,  $\text{CsTiCl}_3$  exists in two different polymorphs: a tetragonal phase ( $I4/m$ ) and a cubic phase ( $Fm\bar{3}m$ ) [25].

The possible candidates for low-energy crystal structures of  $\text{AlInCl}_3$  have been also investigated along with  $\text{AlInF}_3$ . Since fluorine and chlorine atoms belong to the same halogen group in the periodic table,  $\text{AlInCl}_3$  is expected to have close resemblances to  $\text{AlInF}_3$  structurally and electronically. To check the possible low-energy crystal structures for  $\text{AlInCl}_3$ , we examined the total energies of the crystal structures listed in Fig. 1 and the results are shown in Fig. 3. For both  $\text{LiInCl}_3$  and  $\text{NaInCl}_3$ , four space groups,  $R\bar{3}$ ,  $P\bar{1}-a$ ,  $C2$ , and  $C2/m-c$ , are candidates for the lowest energy structure and have tiny energy differences only within 5 meV/atom. The details of the energy differences could be found in Table II. These four space groups,  $R\bar{3}$ ,  $P\bar{1}-a$ ,  $C2$ , and  $C2/m-c$ , possess two different sizes of  $\text{InCl}_6$  octahedra (bond disproportionation, see Fig. 1), which leads to In having  $\text{In}^{1+}$  and  $\text{In}^{3+}$  valence states and showing charge/valence disproportionation. For  $\text{AlInCl}_3$  ( $A = \text{K}, \text{Rb}, \text{Cs}$ ), two space groups,  $C2/m-b$  and  $P\bar{1}-b$ , are candidates for the lowest energy structure. Energy differences between the two space groups are 7.8, 4.6, and 2.8 meV/atom for K, Rb, and Cs compounds, respectively (see Table II). These two space groups possess symmetrically equivalent In atoms in the unit cell, hence charge/valence disproportionation is not available for these space groups (bond disproportionation is not available as well). The coordination number of In in both  $C2/m-b$  and  $P\bar{1}-b$  space groups is 3, which is quite distinct from the others listed in Fig. 1. The space group  $I4/mmm-a$  has higher energy as the alkali metal gets heavier as shown in Fig. 3. Besides, energy differences among space groups except for  $I4/mmm-a$  are significant for  $\text{LiInCl}_3$  and become smaller as the alkali metal becomes heavier. These two tendencies are also realized in  $\text{AlInF}_3$  compounds (Fig. 2).

### C. Thermodynamic stability

We construct the ternary phase diagrams for  $\text{AlInF}_3$  compounds as shown in Fig. 4. All lowest-energy  $\text{AlInF}_3$  compounds are thermodynamically stable (Table I). The determinant reactions for  $\text{AlInF}_3$  are



Given the above determinant reactions, we can estimate the energy above/below hull ( $E_{\text{Hull}}$ ) for  $\text{AlInF}_3$  and the results are shown in Table I. Since all the lowest-energy  $\text{AlInF}_3$  compounds have substantial energies below hull, they are most likely to form.

We are now in a position to discuss the possibility of synthesis of suggested  $\text{AlInF}_3$  materials. To do that, we made a probabilistic model to estimate the existence probability of a material [31]. If a material has a significant energy below hull, the existence probability becomes larger, indicating synthesis of the material would be likely possible.  $\text{LiInF}_3$ ,  $\text{NaInF}_3$ ,  $\text{KInF}_3$ , and  $\text{RbInF}_3$  have energy below hull of -30, -54, -21, and -50 meV/atom, respectively, which correspond to the existence probability of 0.56, 0.64, 0.52, and 0.62, respectively. Since these ex-

TABLE I. Hull energy ( $E_{\text{Hull}}$ ), energy difference ( $\Delta E$ ), and existence probability for the low-energy crystal structure of  $\text{AlInF}_3$  ( $A = \text{alkali metals}$ ). The hull energy is obtained from the determinant reaction (see text), the energy difference is estimated with respect to the crystal structure having the lowest energy, and the existence probability is calculated by using the probabilistic model introduced in Ref. [31]. The units for  $E_{\text{Hull}}$  and  $\Delta E$  are meV/atom.

Space group	$E_{\text{Hull}}$ (meV)	$\Delta E$ (meV)	Prob.
<b>LiInF<sub>3</sub></b>			
$I4/mmm-a$ (No. 139)	-30.362	0	0.56
$R\bar{3}$ (No. 148)	14.860	45.222	0.39
<b>NaInF<sub>3</sub></b>			
$I4/mmm-a$ (No. 139)	-54.183	0	0.64
$P\bar{1}-b$ (No. 2)	-33.838	20.345	0.57
<b>KInF<sub>3</sub></b>			
$I4/mmm-b$ (No. 139)	-20.501	0	0.52
$P\bar{1}-b$ (No. 2)	-7.298	13.202	0.46
<b>RbInF<sub>3</sub></b>			
$I4/mmm-b$ (No. 139)	-49.727	0	0.62
$C2/m-a$ (No. 12)	-39.139	10.588	0.59
$P\bar{1}-a$ (No. 2)	-39.109	10.618	0.59
<b>CsInF<sub>3</sub></b>			
$C2/m-a$ (No. 12)	-115.011	0	0.78
$I4/m$ (No. 87)	-114.999	0.012	0.78
$R\bar{3}$ (No. 148)	-114.995	0.016	0.78
$P\bar{1}-a$ (No. 2)	-114.983	0.028	0.78
$Fm\bar{3}m$ (No. 225)	-114.228	0.783	0.77

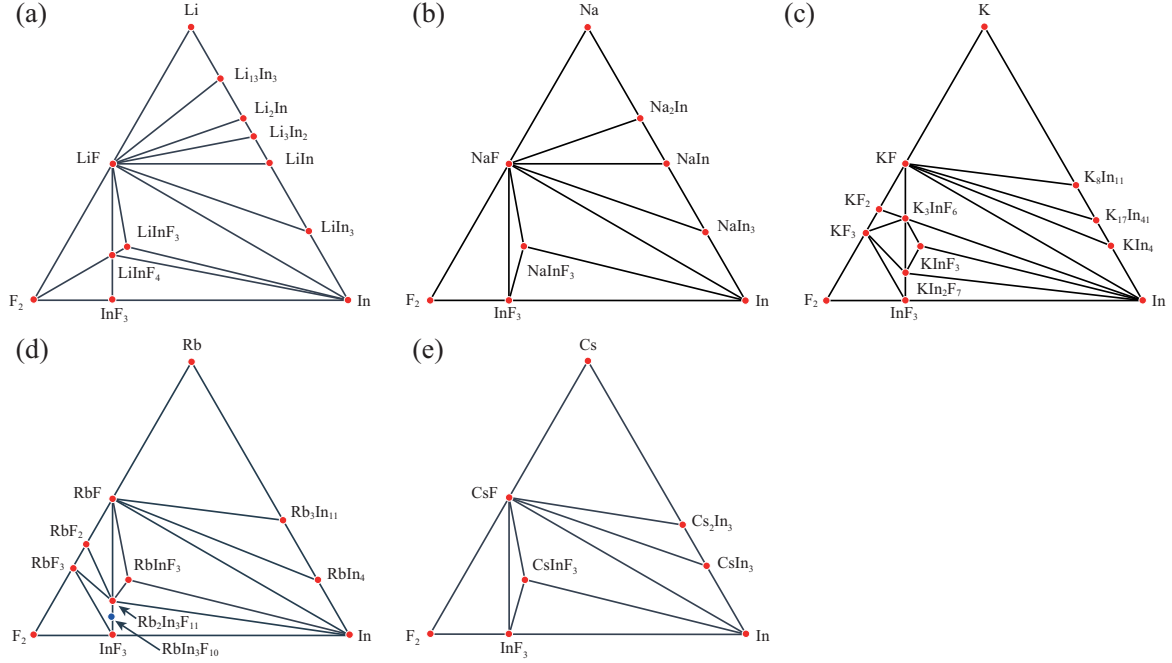
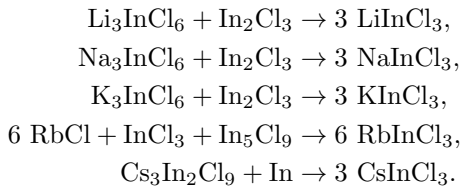


FIG. 4. (Color Online) Ternary phase diagrams for (a)  $\text{LiInF}_3$ , (b)  $\text{NaInF}_3$ , (c)  $\text{KInF}_3$ , (d)  $\text{RbInF}_3$ , and (e)  $\text{CsInF}_3$ . Note that  $\text{RbIn}_3\text{F}_{10}$  is marginally stable with a tiny energy above hull of 1.26 meV/atom (existence probability of 0.43).

istence probabilities are large enough, these  $\text{AInF}_3$  compounds are expected to be synthesized in laboratory. Especially  $\text{CsInF}_3$  phases have energies below hull of order of -100 meV/atom, which corresponds to the existence probability of 0.78. Since five candidate structures have small energy differences among them (within 1 meV/atom), existence probabilities for the structures are almost same as 0.78 (see Table. I). As mentioned before, the synthesis of the crystal structure strongly depends on the synthesis method and condition. In the case of  $\text{CsInF}_3$ , one of the five candidate structures would be chosen and synthesized depending on the synthesis condition. Otherwise, the material exists in several different polymorphs.

Figure 5 shows the ternary phase diagrams for  $\text{AInCl}_3$  compounds. The determinant reactions for  $\text{AInCl}_3$  are



Given the above determinant reactions, we can estimate the energy above/below hull ( $E_{\text{Hull}}$ ) for  $\text{AInCl}_3$  and the results are shown in Table II. All the lowest-energy  $\text{AInCl}_3$  compounds are thermodynamically stable except for  $\text{KInCl}_3$ .  $\text{KInCl}_3$  has energy above hull of 0.617 meV/atom and the corresponding existence probability is 0.43, which is quite significant. Therefore,  $\text{KInCl}_3$  is marginally stable and is still expected to be synthesized in laboratory. The other  $\text{AInCl}_3$  compounds have en-

ergy below hull of -23, -4, -79, and -20 meV/atom for Li, Na, Rb, and Cs compounds, which correspond to the existence probability of 0.53, 0.45, 0.70, and 0.52, respectively. Since these existence probabilities are large enough, these  $\text{AInCl}_3$  compounds are expected to be synthesized in laboratory. Both  $\text{LiInCl}_3$  and  $\text{NaInCl}_3$  have tiny energy differences (within 5 meV/atom) among four

TABLE II. Same as Table. I for  $\text{AInCl}_3$  compounds.

Space group	$E_{\text{Hull}}$ (meV)	$\Delta E$ (meV)	Prob.
<b>LiInCl<sub>3</sub></b>			
<i>C</i> 2 (No. 5)	-23.532	0	0.53
<i>C</i> 2/ <i>m-c</i> (No. 12)	-23.228	0.304	0.53
<i>R</i> 3̄ (No. 148)	-21.669	1.863	0.52
<i>P</i> 1̄- <i>a</i> (No. 2)	-21.648	1.885	0.52
<b>NaInCl<sub>3</sub></b>			
<i>C</i> 2 (No. 5)	-4.727	0	0.45
<i>C</i> 2/ <i>m-c</i> (No. 12)	-3.410	1.316	0.45
<i>R</i> 3̄ (No. 148)	0.114	4.841	0.44
<i>P</i> 1̄- <i>a</i> (No. 2)	0.130	4.857	0.44
<b>KInCl<sub>3</sub></b>			
<i>C</i> 2/ <i>m-b</i> (No. 12)	0.617	0	0.43
<i>P</i> 1̄- <i>b</i> (No. 2)	8.450	7.833	0.41
<b>RbInCl<sub>3</sub></b>			
<i>P</i> 1̄- <i>b</i> (No. 2)	-79.011	0	0.70
<i>C</i> 2/ <i>m-b</i> (No. 12)	-74.430	4.581	0.69
<b>CsInCl<sub>3</sub></b>			
<i>P</i> 1̄- <i>b</i> (No. 2)	-20.112	0	0.52
<i>C</i> 2/ <i>m-b</i> (No. 12)	-17.336	2.776	0.51
<i>I</i> 4/ <i>m</i> (No. 87)	-11.657	8.455	0.48

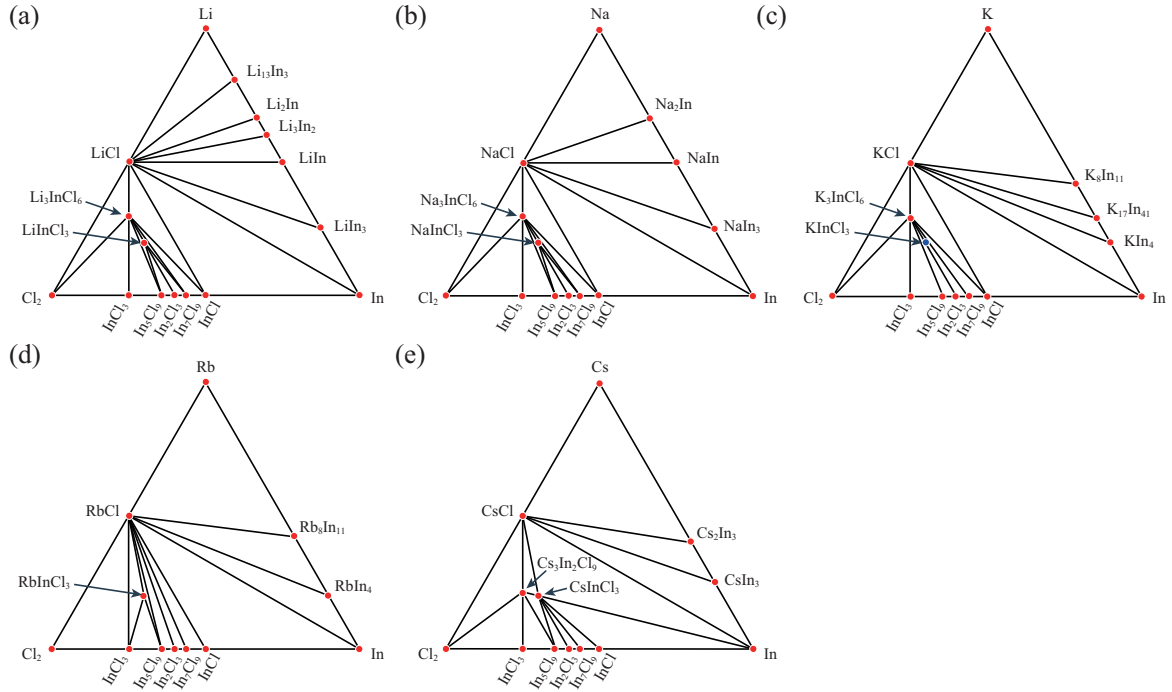


FIG. 5. (Color Online) Ternary phase diagrams for (a)  $\text{LiInCl}_3$ , (b)  $\text{NaInCl}_3$ , (c)  $\text{KInCl}_3$ , (d)  $\text{RbInCl}_3$ , and (e)  $\text{CsInF}_3$ . Red and blue filled circles represent thermodynamically stable and unstable phases, respectively.  $\text{KInCl}_3$  is thermodynamically unstable with a quite small energy above hull of 0.617 meV/atom, which is marginally stable.

candidate space groups,  $C2$ ,  $C2/m-c$ ,  $R\bar{3}$ , and  $P\bar{1}-a$ . For  $\text{RbInCl}_3$  and  $\text{CsInCl}_3$ , two candidate space groups,  $P\bar{1}-b$  and  $C2/m-b$ , also have tiny energy differences (within 5 meV/atom) between them. Therefore  $\text{AInCl}_3$  ( $A = \text{Li, Na, Rb, Cs}$ ) could be synthesized into one of the candidate structures depending on the synthesis condition. Otherwise, the material exists in several different polymorphs. For  $\text{CsInCl}_3$ , the third lowest-energy structure ( $I4/m$ ) has a small energy difference of  $\sim 8$  meV with the lowest one and still has a possibility to form due to the considerable existence probability of 0.48 as shown in Table. II.

#### D. Electronic structure and superconductivity

We have calculated the electronic structures of  $\text{AInF}_3$  compounds and found several similarities and differences among them. In Fig. 6, we present two representative electronic structures of  $I4/mmm-a$   $\text{LiInF}_3$  and  $C2/m-a$   $\text{CsInF}_3$ . The similarities and differences in the electronic structures of  $\text{AInF}_3$  will be discussed later.

Figure 6 shows that both  $\text{LiInF}_3$  and  $\text{CsInF}_3$  have an insulating phase with an indirect band gap of 4.37 and 4.06 eV, respectively, based on the mBJ method (GGA results give 2.30 and 3.05 eV, respectively). In addition, In  $s$  and F  $p$  orbitals are well separated in the energy window, which leads to only small hybridization between In  $s$  and F  $p$  orbitals. The only notable hybridization is between In  $s$  and F  $p_\sigma$  orbitals, which produces the

low-lying bonding state located at  $-8 \sim -6$  eV as shown in Fig. 6. However, the low-lying bonding state has dominant F  $p_\sigma$  character and quite small In  $s$  character (see the density of states in Fig. 6). Due to the quite small hybridization between In  $s$  and F  $p$  orbitals, we can mention that  $\text{LiInF}_3$  and  $\text{CsInF}_3$  have  $\text{In}^{2+}$  ( $5s^1$ ) and multivalent  $\text{In}^{1+}$  ( $5s^2$ ) and  $\text{In}^{3+}$  ( $5s^0$ ) configurations, respectively. We would like to note that charge disproportionation in  $\text{BaBiO}_3$  [ $2\text{Bi}^{4+} \rightarrow \text{Bi}^{3+} + \text{Bi}^{5+}$ ] was questioned due to the significant hybridization between Bi  $6s$  and O  $2p$  orbitals. The alternative scenario of oxygen hole pairs condensation ( $2\text{Bi}^{3+}\underline{\text{L}} \rightarrow \text{Bi}^{3+}\underline{\text{L}}^2 + \text{Bi}^{5+}$ , where  $\underline{\text{L}}$  represents a ligand hole) was proposed [63–65]. In the case of  $\text{CsInF}_3$ , however, hybridization between In  $s$  and F  $p$  orbitals is quite small. Hence, the ligand hole pairs condensation scenario is safely ruled out and valence/charge disproportionation is clearly realized.

The electronic structures of other low-energy  $\text{AInF}_3$  compounds including  $I4/mmm-a$   $\text{NaInF}_3$ ,  $I4/mmm-b$   $\text{KInF}_3$ , and  $I4/mmm-b$   $\text{RbInF}_3$  (not shown) are quite similar to that of  $I4/mmm-a$   $\text{LiInF}_3$  except for the different size of the band gap. The sizes of the indirect band gap for Na, K, and Rb compounds obtained from the mBJ method are 3.89, 3.91, and 3.67 eV, (GGA results give 1.77, 1.90, and 1.90 eV), respectively, which are smaller than that for  $\text{LiInF}_3$ . For  $\text{CsInF}_3$ , the five candidate structures, which are  $C2/m-a$ ,  $I4/m$ ,  $R\bar{3}$ ,  $P\bar{1}-a$ , and  $Fm\bar{3}m$ , also have similar electronic structure in the following manner: (i) In  $s$  and F  $p$  orbitals are well separated in the energy window (In  $s$  and F  $p$  orbitals lie

-1 ~ 7 eV and -7 ~ -4 eV, respectively), (ii) quite small hybridization between In  $s$  and F  $p$  orbitals is realized, (iii) multivalent  $\text{In}^{1+}$  ( $5s^2$ ) and  $\text{In}^{3+}$  ( $5s^0$ ) valence skip configuration is clearly shown, and (iv) the five candidate structures have similar band gaps of ~4.0 eV (GGA results give almost same band gaps of ~3.0 eV).

Both  $I4/mmm$ -a  $\text{LiInF}_3$  and  $C2/m$ -a  $\text{CsInF}_3$  show an insulating behavior, however, the insulating mechanism is different (The insulating mechanism of the Na, K, and Rb compounds is essentially same as the Li compound). As shown in Fig. 6(b),  $C2/m$ -a  $\text{CsInF}_3$  exhibits the mix-valent  $\text{In}^{1+}$  ( $5s^2$ ) and  $\text{In}^{3+}$  ( $5s^0$ ) character [66], where  $\text{In}^{1+}$  has a completely filled  $s$ -band and  $\text{In}^{3+}$  has an (nearly) empty  $s$ -band (there is a small amount of  $\text{In}^{3+}$   $s$ -orbital character in the occupied band due to the small hybridization between In  $s$  and F  $p_\sigma$  orbitals). Therefore, the insulating mechanism in  $C2/m$ -a  $\text{CsInF}_3$  is straightforward: the mix-valent character makes the insulating phase. For the case of  $I4/mmm$ -a  $\text{LiInF}_3$ ,  $\text{In}^{2+}$  ( $5s^1$ ) character is clearly shown in Fig. 6(a), where  $\text{In}^{2+}$  has the half-filled  $s$ -band, which is not straightforward to understand the band gap formation. In order to investigate the insulating mechanism in  $I4/mmm$ -a  $\text{LiInF}_3$  thoroughly, we plot the charge density with the energy range between -2 and 0 eV (the Fermi level is set to be zero) in Fig. 7(b), which corresponds to the  $ss\sigma$ -bonding character. Therefore, two adjacent In atoms are dimerized with the bond length of 2.75 Å to produce  $ss\sigma$  (bonding) and  $ss\sigma^*$  (anti-bonding) states, and each  $s$ -electron in  $\text{In}^{2+}$  completely fills the  $ss\sigma$ -bonding state (Fig. 7(a)). The band gap size

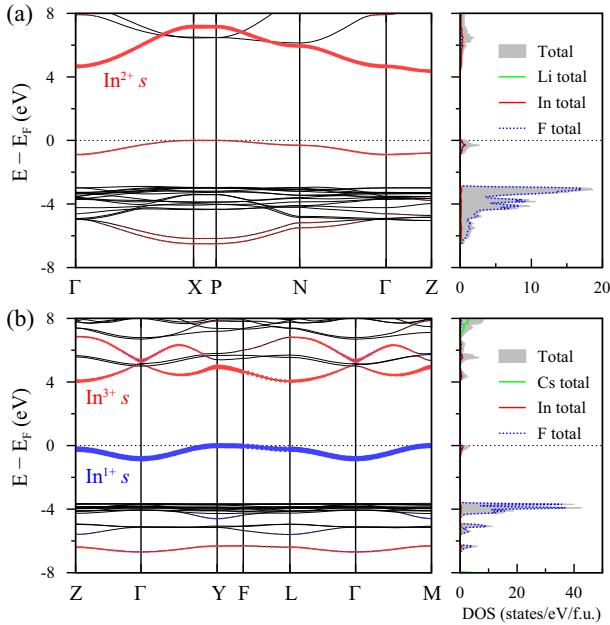


FIG. 6. (Color Online) Electronic structures of (a)  $I4/mmm$ -a  $\text{LiInF}_3$  and (b)  $C2/m$ -a  $\text{CsInF}_3$  calculated by the mBJ method.  $\text{In}^{2+}$   $s$ -orbital character is marked in red in (a) and  $\text{In}^{3+}$  and  $\text{In}^{1+}$   $s$ -orbital characters are marked in red and blue in (b), respectively, in the band structures.

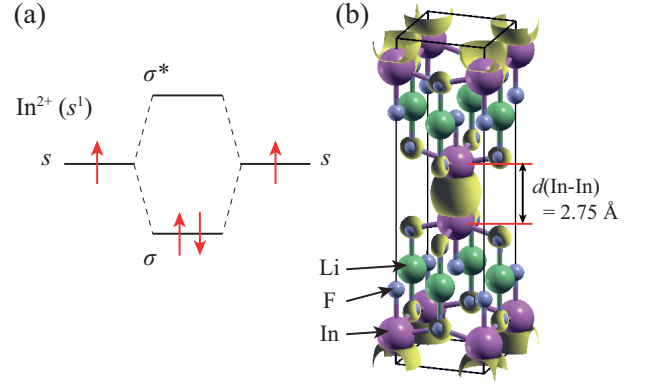


FIG. 7. (Color Online) Insulating mechanism of  $I4/mmm$ - $\text{LiInF}_3$ . (a) Systematic band diagram for a band gap opening. Two  $s$  orbitals from two adjacent  $\text{In}^{2+}$  atoms form  $ss\sigma$ -bonding to open the band gap. (b) Electronic charge density corresponding to the  $ss\sigma$ -bonding. The distance between two adjacent  $\text{In}^{2+}$  atoms is 2.75 Å.

in  $I4/mmm$ -a  $\text{LiInF}_3$  indicates the splitting between  $ss\sigma$  (bonding) and  $ss\sigma^*$  (anti-bonding) states.

The electronic structures of all  $\text{AlInCl}_3$  compounds show insulating behavior as well (not shown).  $\text{AlInCl}_3$  could be classified into two groups:  $\text{LiInCl}_3$  and  $\text{NaInCl}_3$  are in the same group and  $\text{KInCl}_3$ ,  $\text{RbInCl}_3$ , and  $\text{CsInCl}_3$  belong to the other group. For each group, they share the same low-energy candidate structures: both  $\text{LiInCl}_3$  and  $\text{NaInCl}_3$  have four candidate structures with space groups of  $C2$ ,  $C2/m$ -c,  $R\bar{3}$ , and  $P\bar{1}$ -a, and  $\text{KInCl}_3$ ,  $\text{RbInCl}_3$ , and  $\text{CsInCl}_3$  have two candidate structures with space groups of  $P\bar{1}$ -b and  $C2/m$ -b. Not only the electronic structures but also the size of the band gap are almost the same among the candidate structures for each  $\text{AlInCl}_3$  compound. The band gaps obtained from the mBJ method are 3.5, 3.5, 4.2, 4.3, and 4.3 eV for Li, Na, K, Rb, and Cs compounds, respectively (GGA gives the band gaps of 2.8, 2.7, 2.9, 3.0, and 3.0 eV, respectively). For both  $\text{LiInCl}_3$  and  $\text{NaInCl}_3$ , their four candidate structures possess two different sizes of  $\text{InCl}_6$  octahedra (bond disproportionation) and show the multivalent  $\text{In}^{1+}$  ( $5s^2$ ) and  $\text{In}^{3+}$  ( $5s^0$ ) valence skip configuration. Note that In  $s$  and Cl  $p$  orbitals are well separated in the energy window and only a small hybridization between In  $s$  and Cl  $p_\sigma$  orbitals is somewhat bigger than that between In  $s$  and F  $p_\sigma$  orbitals. However, the hybridization between In  $s$  and Cl  $p$  is still quite small, hence the ligand hole pairs condensation scenario is safely ruled out and valence/charge disproportionation is clearly realized. Interestingly, two  $s$  bands originating from  $\text{In}^{1+}$  and  $\text{In}^{3+}$  atoms are almost flat (their bandwidths are smaller than 1 eV) and are located at near the Fermi level and ~4 eV, respectively. For  $\text{KInF}_3$ ,  $\text{RbInF}_3$ , and  $\text{CsInF}_3$  compounds, their candidate structures with space groups of  $P\bar{1}$ -b and  $C2/m$ -b have symmetrically equivalent In



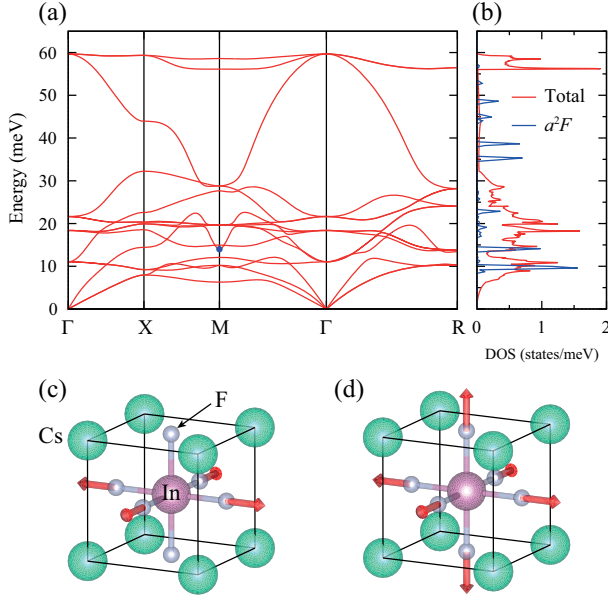


FIG. 8. (Color Online) (a) Phonon dispersion and (b) the corresponding phonon density of state and the Eliashberg function  $a^2F(\omega)$  of 0.5 hole-doped cubic  $Pm\bar{3}m$ -CsInF<sub>3</sub> under pressure  $P = 32$  GPa ( $a = 4.233$  Å). The unit cell of cubic  $Pm\bar{3}m$ -CsInF<sub>3</sub> is shown in (c) and (d). The arrows in (c) and (b) show phonon normal modes at  $q = M$  and  $R$ , respectively, having a significant electron-phonon coupling constant. The phonon normal mode having the largest electron-phonon coupling strength  $\lambda_{q\nu}$  is the F stretching phonon mode shown in (c) and the size of  $\lambda_{q\nu}$  is marked by a blue circle in (a).

atoms in the unit cell. Therefore, valence/charge disproportionation is not possible in their candidate structures. Alkali metal (K, Rb, Cs) and Cl atoms strongly prefer the valence states of 1+ and 1-, respectively, leading to In atoms having 2+ valence state. The insulating mechanism of these compounds is essentially the same as the one discussed in LiInF<sub>3</sub>, and the band gap is formed between the fully occupied  $ss\sigma$  bonding and totally empty  $ss\sigma^*$  anti-bonding states.

As discussed earlier, all AInX<sub>3</sub> (A = alkali metals, X = F or Cl) compounds have insulating behavior with a significant band gap of approximately 4 eV (based on the mBJ method). Hence, these compounds are not suitable for photovoltaic materials (appropriate band gap size is ranged from 1 to 2 eV) without any band gap tuning like, for example, applying strain or pressure.

Now, we discuss the possible superconductivity in these new In compounds. As shown in Fig. 6, hole doping gives the higher electronic density of states than electron doping in both LiInF<sub>3</sub> and CsInF<sub>3</sub>. Therefore, hole doping would be expected to give higher superconducting transition temperature  $T_c$  than electron doping.

We calculated the electron-phonon coupling constant  $\lambda$  in 10 % hole-doped  $I4/mmm$ -a LiInF<sub>3</sub>. We found that  $\lambda = 0.324$  and the logarithmic average phonon frequency  $\omega_{log} = 304$  K, which gives the superconducting transi-

TABLE III. Phonon related physical parameters for 0.5 hole-doped simple cubic CsInF<sub>3</sub> under pressure  $P = 32$  GPa. The reduced electron-phonon matrix element (REPME), the total electron-phonon coupling  $\lambda$ , the average phonon frequency  $\omega_{log}$ , and the superconducting transition temperature  $T_c$  are evaluated in both GGA and HSE06 methods. The REPME is obtained for the F stretching mode shown in Fig. 8(c), which is the most important vibration mode. The temperature  $T_c$  is estimated by using the McMillan-Allen-Dynes formula [68] with  $\mu^* = 0.10$ .  $T_c$  with  $\mu^* = 0.15$  is also provided in the parentheses. Note that the temperature  $T_c$  is not sensitive to  $\mu^*$  within the confidence interval ranged from 0.10 to 0.15.

	GGA	HSE06
REPME (eV/Å)	5.00	6.95
$\lambda$	1.80	3.48
$\omega_{log}$ (K)	157	124
$T_c$ (K)	21 (18)	24 (22)

tion temperature  $T_c = 0.293$  (0.02) K when we use the effective Coulomb repulsion parameter  $\mu^* = 0.10$  (0.15) in the McMillan-Allen-Dynes formula [68].

The emergence of superconductivity was reported in charged doped cubic perovskite BaBiO<sub>3</sub> [56] and CsTiX<sub>3</sub> (X = F or Cl) [26] materials. Therefore, the simple cubic perovskite CsInF<sub>3</sub> ( $Pm\bar{3}m$ ; No. 221) is also tested for possible superconductivity. At ambient pressure, it is mechanically unstable with imaginary phonon softening at  $X$  and  $R$  points (not shown) even with sufficient doping. The unstable phonon mode at  $R$  point is the InF<sub>6</sub> octahedron breathing mode as shown in Fig. 8(d). With sufficient doping and at high pressure, the structure distortions and valence disproportionation realized in CsInF<sub>3</sub> (the second row of Fig. 1) could be suppressed and CsInF<sub>3</sub> could crystallize in the simple cubic perovskite structure accompanied by a transition to the metallic phase. This bears a close resemblance to the phase diagram of BaBiO<sub>3</sub> [59, 61].

Figure 8(a) shows the phonon dispersion of 0.5 hole-doped cubic perovskite CsInF<sub>3</sub> under pressure of  $P = 32$  GPa (hole-doped CsInF<sub>3</sub> is possible through a certain amount of oxygen substitution for fluorine, for example, CsIn(F<sub>1-x</sub>O<sub>x</sub>)<sub>3</sub>, or Cs vacancy could introduce hole doping). The F vibrational mode has the highest energy due to its small mass. However, at particular phonon momentum  $q$  (especially at  $q = M, R$ ), this F vibrational mode shows quite significant phonon softening indicating fairly large electron-phonon coupling. The phonon momentum  $q$  and mode  $\nu$  dependent electron-phonon coupling strength  $\lambda_{q\nu}$  are 7.24 and 0.19 for the soft phonon modes shown in Figs. 8(c) and (d), respectively. The (total) electron-phonon coupling constant  $\lambda$  is 1.80 and the logarithmic average phonon frequency  $\omega_{log} = 157$  K. The McMillan-Allen-Dynes formula [68] with  $\mu^* = 0.10$  (0.15) gives  $T_c = 21$  (18) K.

Conventional electronic descriptions based on LDA/GGA underestimates the electron-phonon coupling constant  $\lambda$  in Ba<sub>1-x</sub>K<sub>x</sub>BiO<sub>3</sub> and fail to explain

its high-temperature superconductivity [69]. Yin *et al.* found that static correlation (which is captured within GW or the hybrid HSE06 functional) enhances the electron-phonon coupling constant  $\lambda$  and describes the transition temperature  $T_c$  properly [56]. Motivated by the above study [56], the effect of static correlation on superconductivity in  $\text{CsInF}_3$  is also tested. Since the F stretching phonon mode (Fig. 8(c)) is the most important to account for superconductivity, we calculated a reduced electron-phonon matrix element (REPME) [56] for the phonon mode. Table III shows that static correlation enhances the REPME by a factor of  $\sim 1.4$  and gives rise to larger electron-phonon coupling constant  $\lambda = 3.48$  and  $T_c \approx 24$  K. These results encourage the pursuit of experimental synthesis.

## V. SUMMARY AND CONCLUSIONS

Using computational methods we identified nine new In compounds  $\text{AlnX}_3$  ( $A = \text{alkali metals}$ ,  $X = \text{F or Cl}$ ) and investigated their crystal structures and physical properties. Two distinct insulating mechanisms are realized in the new In compounds. For the compounds that have different sizes of  $\text{InX}_6$  octahedra (bond disproportionation), which are  $\text{CsInF}_3$ ,  $\text{LiInCl}_3$ , and  $\text{NaInCl}_6$ , they show multivalent  $\text{In}^{3+}$  ( $5s^0$ ) and  $\text{In}^{1+}$  ( $5s^2$ ) valence skip configuration. The insulating phase is induced from bond and valence disproportionation. The other In compounds,  $\text{AlnF}_3$  ( $A = \text{Li, Na, K, Rb}$ ) and  $\text{AlnCl}_3$  ( $A = \text{K, Rb, Cs}$ ), have symmetrically equivalent In sites in their unit cell and hence both bond and valence disproportionation are not possible. These In compounds have the divalent valence state of In, which is very rare but thermodynamically stable. In these compounds, two adjacent In atoms are dimerized to produce  $ss\sigma$  bonding and  $ss\sigma^*$  antibonding states. Each  $s$ -electron in  $\text{In}^{2+}$  completely fills the  $ss\sigma$  bonding states. Therefore, the band gap sizes in these compounds indicate the splitting between  $ss\sigma$  bonding and  $ss\sigma^*$  antibonding states.

These compounds are a new arena for investigating charge, valence, and bond disproportionation. They are similar to the  $\text{CsTiX}_3$  ( $X = \text{F or Cl}$ ), which had also been predicted theoretically and synthesized experimentally [25, 26], but do not have the toxicity problems associated with Tl, and therefore can be synthesized more easily. All these  $\text{AlnX}_3$  compounds are insulators with a sizable indirect band gap of the order of  $\sim 4$  eV, which makes them unsuitable for photovoltaic materials. We also studied the possible superconductivity in these new In compounds. With sufficient doping and at high pressure,  $\text{CsInF}_3$  crystallizes in the simple cubic perovskite structure and has a significant superconducting transition temperature of  $T_c \approx 24$  K.

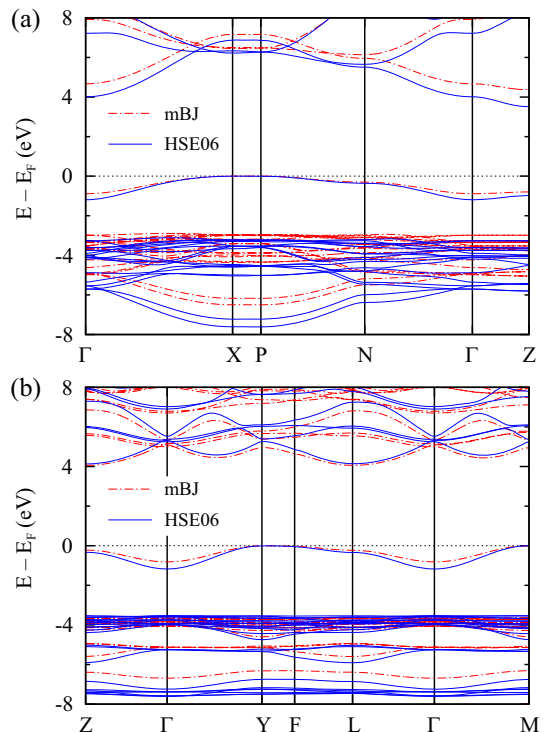


FIG. 9. (Color Online) Comparison between mBJ and HSE06 methods for (a)  $I4/mmm$ -a  $\text{LiInF}_3$  and (b)  $C2/m$ -a  $\text{CsInF}_3$ . Both mBJ and HSE06 methods give the similar band gap.

## ACKNOWLEDGMENTS

We thank Ran Adler, Ian Fisher, Martha Greenblatt, and Xiaoyan Tan for fruitful discussions. This work was supported by the Air Force Office of Scientific Research supported MURI under Grant No. FA9550-14-1-0331.

## VI. APPENDIX

We have estimated the band gaps of the semiconducting systems within the mBJ method. In Appendix, we discuss the computational validity of the mBJ method. For the semiconducting systems, the mBJ method is efficient to improve the band gap but is empirical. On the other hand, the rather computationally expensive HSE06 method is well physically constructed and is more accurate on this aspect. Here, we compute the electronic structure within the HSE06 method and compare it with the mBJ method.

Figure 9 shows a comparison between the mBJ and HSE06 methods for two representative electronic structures of  $I4/mmm$ -a  $\text{LiInF}_3$  and  $C2/m$ -a  $\text{CsInF}_3$ . For  $I4/mmm$ -a  $\text{LiInF}_3$ , mBJ and HSE06 methods give indirect band gaps of 4.37 and 3.51 eV, respectively. In addition, both methods give indirect band gaps of 4.06 and 4.15 eV, respectively, for  $C2/m$ -a  $\text{CsInF}_3$ . Since both mBJ and HSE06 methods give a similar band gap for

the semiconducting systems investigated in this study,

the band gaps estimated from the mBJ method are reliable.

- 
- [1] D. Duan, Y. Liu, F. Tian, D. Li, X. Huang, Z. Zhao, H. Yu, B. Liu, W. Tian, and T. Cui, *Sci. Rep.* **4**, 6968 (2014).
- [2] A. P. Drozdov, M. I. Erements, and I. A. Troyan, [arXiv:1412.0460](https://arxiv.org/abs/1412.0460) (2014).
- [3] A. P. Drozdov, M. I. Erements, I. A. Troyan, A. Ksenofontov, and S. I. Shylin, *Nature (London)* **525**, 73 (2015).
- [4] I. Errea, M. Calandra, C. J. Pickard, J. Nelson, R. J. Needs, Y. Li, H. Liu, Y. Zhang, Y. Ma, and F. Mauri, *Phys. Rev. Lett.* **114**, 157004 (2015).
- [5] Y. Ge, F. Zhang, and Y. Yao, *Phys. Rev. B* **93**, 224513 (2016).
- [6] J. H. Shim, K. Haule, and G. Kotliar, *Phys. Rev. B* **79**, 060501(R) (2009).
- [7] N. Katayama, K. Kudo, S. Onari, T. Mizukami, K. Sugawara, Y. Sugiyama, Y. Kitahama, K. Iba, K. Fujimura, N. Nishimoto, M. Nohara, and H. Sawa, *J. Phys. Soc. Jpn.* **82**, 123702 (2013).
- [8] C.-J. Kang, T. Birol, and G. Kotliar, *Phys. Rev. B* **95**, 014511 (2017).
- [9] X. Zhang, L. Yu, A. Zakutayev, and A. Zunger, *Adv. Funct. Mater.* **22**, 1425 (2012).
- [10] F. Yan, X. Zhang, Y. G. Yu, L. Yu, A. Nagaraja, T. O. Mason, and A. Zunger, *Nat. Commun.* **6**, 7308 (2015).
- [11] R. Gautier, X. Zhang, L. Hu, L. Yu, Y. Lin, T. O. L. Sunde, D. Chon, K. R. Poeppelmeier, and A. Zunger, *Nat. Chem.* **7**, 308 (2015).
- [12] Q. Hu, D. Y. Kim, W. Yang, L. Yang, Y. Meng, L. Zhang, and H.-K. Mao, *Nature* **534**, 241 (2016).
- [13] Y.-L. Li, S.-N. Wang, A. R. Oganov, H. Gou, J. S. Smith, and T. A. Strobel, *Nat. Commun.* **6**, 6974 (2015).
- [14] X. Dong, A. R. Oganov, A. F. Goncharov, E. Stavrou, S. Lobanov, G. Saleh, G.-R. Qian, Q. Zhu, C. Gatti, V. L. Deringer, R. Dronskowski, X.-F. Zhou, V. B. Prakapenka, Z. Konôpková, I. A. Popov, A. I. Boldyrev, and H.-T. Wang, *Nat. Chem.* **9**, 440 (2017).
- [15] S. Curtarolo, G. L. W. Hart, M. B. Nardelli, N. Mingo, S. Sanvito, and O. Levy, *Nat. Mater.* **12**, 191 (2013).
- [16] J. E. Saal, S. Kirklin, M. Aykol, B. Meredig, and C. Wolverton, *JOM* **65**, 1501 (2013).
- [17] K. T. Butler, J. M. Frost, J. M. Skelton, K. L. Svane, and A. Walsh, *Chem. Soc. Rev.* **45**, 6138 (2016).
- [18] A. Jain, Y. Shin, and K. A. Persson, *Nat. Rev. Matter.* **1**, 15004 (2016).
- [19] A. Jain, K. A. Persson, and G. Ceder, *APL Mater.* **4**, 053102 (2016).
- [20] K. T. Butler, D. W. Davies, H. Cartwright, O. Isayev, and A. Walsh, *Nature* **559**, 547 (2018).
- [21] C. M. Varma, *Rev. Mod. Phys.* **48**, 219 (1976).
- [22] G. E. Eperon, G. M. Paternò, R. J. Sutton, A. Zampetti, A. A. Haghighirad, F. Cacialli, and H. J. Snaith, *J. Mater. Chem. A* **3**, 19688 (2015). (DOI: 10.1039/c5ta06398a)
- [23] M. R. Filip and F. Giustino, *J. Phys. Chem. C* **120**, 166 (2016).
- [24] S. Körbel, M. A. L. Marques, and S. Botti, *J. Mater. Chem. C* **4**, 3157 (2016).
- [25] M. Retuerto, T. Emge, J. Hadermann, P. W. Stephens, M. R. Li, Z. P. Yin, M. Croft, A. Ignatov, S. J. Zhang, Z. Yuan, C. Jin, J. W. Simonson, M. C. Aronson, A. Pan, D. N. Basov, G. Kotliar, and M. Greenblatt, *Chem. Mater.* **23**, 4071 (2013).
- [26] Z. P. Yin and G. Kotliar, *EPL* **101**, 27002 (2013).
- [27] R. J. Cava, B. Batlogg, J. J. Krajewski, R. Farrow, L. W. Rupp Jr, A. E. White, K. Short, W. F. Peck, and T. Kometani, *Nature* **332**, 814 (1988).
- [28] J. A. J. Pardoe and A. J. Downs, *Chem. Rev.* **107**, 2 (2007).
- [29] P. P. Fedorov, A. I. Popov, and R. L. Simoneaux, *Russ. Chem. Rev.* **86**, 240 (2017). (doi: 10.1070/RCR4609)
- [30] R. L. Davidovich, P. P. Fedorov, and A. I. Popov, *Rev. Inorg. Chem.* **36**, 105 (2016). (doi: 10.1515/revic-2015-0019)
- [31] R. Adler, C.-J. Kang, C.-H. Yee, and G. Kotliar, *Rep. Prog. Phys.* in press (2018). (<https://doi.org/10.1088/1361-6633/aadca4>)
- [32] S. M. Woodley and R. Catlow, *Nat. Mater.* **7**, 937 (2008).
- [33] A. Jain, S. P. Ong, G. Hautier, W. Chen, W. D. Richards, S. Dacek, S. Cholia, D. Gunter, D. Skinner, G. Ceder, and K. A. Persson, *APL Materials* **1**, 011002 (2013).
- [34] <https://www.materialsproject.org/>
- [35] S. Kirklin, J. E. Saal, B. Meredig, A. Thompson, J. W. Doak, M. Aykol, S. Rühl, and C. Wolverton, *npj Computational Materials* **1**, 15010 (2015). (doi:10.1038/npjcompumats.2015.10)
- [36] <http://www.oqmd.org/>
- [37] W. Setyawan, R. M. Gaume, S. Lam, R. S. Feigelson, and S. Curtarolo, *ACS Comb. Sci.* **13**, 382 (2011).
- [38] <http://aflowlib.org/>
- [39] A. R. Oganov and C. W. Glass, *J. Chem. Phys.* **124**, 244704 (2006).
- [40] C. W. Glass, A. R. Oganov, and N. Hansen, *Comput. Phys. Commun.* **175**, 713 (2006).
- [41] G. Kresse and J. Furthmüller, *Comput. Mater. Sci.* **6**, 15 (1996).
- [42] G. Kresse and J. Furthmüller, *Phys. Rev. B* **54**, 11169 (1996).
- [43] J. P. Perdew, K. Burke, and M. Ernzerhof, *Phys. Rev. Lett.* **77**, 3865 (1996).
- [44] P. E. Blöchl, *Phys. Rev. B* **50**, 17953 (1994).
- [45] G. Kresse and D. Joubert, *Phys. Rev. B* **59**, 1758 (1999).
- [46] G. Hautier, S. P. Ong, A. Jain, C. J. Moore, and G. Ceder, *Phys. Rev. B* **85**, 155208 (2012).
- [47] L. Wang, T. Maxisch, and G. Ceder, *Phys. Rev. B* **73**, 195107 (2006).
- [48] A. Jain, G. Hautier, S. P. Ong, C. J. Moore, C. C. Fischer, K. A. Persson, and G. Ceder, *Phys. Rev. B* **84**, 045115 (2011).
- [49] S. P. Ong, L. Wang, B. Kang, and G. Ceder, *Chem. Mater.* **20**, 1798 (2008).
- [50] P. Blaha, K. Schwarz, G. K. H. Madsen, D. Kvasnicka, and J. Luitz, *Wien2k* (Karlheinz Schwarz, Technische Universität Wien, Austria, 2001).
- [51] F. Tran and P. Blaha, *Phys. Rev. Lett.* **102**, 226401

- (2009).
- [52] S. Baroni, S. de Gironcoli, A. D. Corso, and P. Giannozzi, *Rev. Mod. Phys.* **73**, 515 (2001).
  - [53] P. Giannozzi *et al.*, *J. Phys. Condens. Matter* **21**, 395502 (2009).
  - [54] K. Lejaeghere *et al.*, *Science* **351**, 1415 (2016).
  - [55] <http://materialscloud.org/sssp/>
  - [56] Z. P. Yin, A. Kutepov, and G. Kotliar, *Phys. Rev. X* **3**, 021011 (2013).
  - [57] A. V. Krukau, O. A. Vydrov, A. F. Izmaylov, and G. E. Scuseria, *J. Chem. Phys.* **125**, 224106 (2006).
  - [58] We have performed USPEX simulations for several  $\text{AlInX}_3$  materials including  $\text{LiInF}_3$ ,  $\text{RbInF}_3$ ,  $\text{CsInF}_3$ ,  $\text{LiInCl}_3$ ,  $\text{RbInCl}_3$ , and  $\text{CsInCl}_3$ . After the USPEX simulations, we have collected the crystal structures with energy differences from the lowest energy within 10 meV/atom for each material and made a structure set as shown in Fig. 1.
  - [59] D. E. Cox and A. W. Sleight, *Solid State Commun.* **19**, 969 (1976).
  - [60] G. Thornton and A. J. Jacobson, *Acta Cryst.* **B34**, 351 (1978).
  - [61] D. E. Cox and A. W. Sleight, *Acta Cryst.* **B35**, 1 (1979).
  - [62] A. F. Orchard and G. Thornton, *J. Chem. Soc. Dalton Trans.* **0**, 1238 (1977).
  - [63] K. Foyevtsova, A. Khazraie, I. Elfimov, and G. A. Sawatzky, *Phys. Rev. B* **91**, 121114(R) (2015).
  - [64] A. Khazraie, K. Foyevtsova, I. Elfimov, and G. A. Sawatzky, *Phys. Rev. B* **97**, 075103 (2018).
  - [65] G. M. Dalpian, Q. Liu, J. Varignon, M. Bibes, and A. Zunger, *Phys. Rev. B* **98**, 075135 (2018).
  - [66] The charge density difference between  $\text{In}^{1+}$  and  $\text{In}^{3+}$  atoms in  $C2/m$ - $\text{CsInF}_3$  is small ( $\sim 0.21 e$ ) in the DFT calculations. Note that there is no real difference in  $d$  occupations even in well-known charge-order transition metal oxides. See Ref. [67] in more detail.
  - [67] Y. Quan, V. Pardo, and W. E. Pickett, *Phys. Rev. Lett.* **109**, 216401 (2012).
  - [68] P. B. Allen and R. C. Dynes, *Phys. Rev. B* **12**, 905 (1975).
  - [69] V. Meregalli and S. Y. Savrasov, *Phys. Rev. B* **57**, 14453 (1998).